Dhaka Univ. J. Sci. 68(2): 111-116, 2020 (July)

Effect of Y^{3+} Substitution on Structural and Magnetic Properties of $Ni_{0.25}Zn_{0.75}Y_xFe_{2-x}O_4$

Sharmin Akhter[1], Probal Roy[1*], Armin Anwar[2], M. A. Hossain[1], M. N. I. Khan[2] and S. S. Sikder[1]

[1]*Department of Physics, Khulna University of Engineering & Technology, Khulna, Bangladesh*
[2]*Department of Physics, University of Dhaka, Dhaka-1000, Bangladesh*
[3]*Materials Science Division, Bangladesh Atomic Energy Commission, Dhaka-1000, Bangladesh*

(Received : 6 November 2019; Accepted : 4 October 2020)

Abstract

The effect of Y^{3+} doping on the structural and magnetic properties of $Ni_{0.25}$ $Zn_{0.75}Y_xFe_{2-x}O_4$ [x= 0.00, 0.02, 0.04, 0.06 and 0.08] was investigated. The specimen was synthesized by conventional solid state reaction method where the sintering temperature was 1150^{o}C for 3 hours. The structure of the specimens was inspected by XRD pattern and SEM micrographs. The XRD patterns delineate the formation of spinel type cubic structure. The lattice parameters, bulk density, X-ray density and porosity were investigated for all the samples. The SEM micrographs shows that the particles of all the composition are within 0.4 – 1.2 μm. M-H curves at room temperature exhibit the ferromagnetic behavior. The effect of Y^{3+} causes drastically variation on saturation magnetization (M_s), coercivity (H_c) and remanent magnetization (M_r). Moreover, the M-H curves delineate the soft ferromagnetic phenomenon which can be the reason of the acceptance of the specimen in industrial applications.

Keywords: Ferrite, Solid state reaction, XRD, SEM, Hysteresis.

I. Introduction

Polycrystalline ferrite materials draw an immense attention in research-oriented fields due to their extensive electrical, magnetic, mechanical and structural phenomenon. The distribution of ferrous and ferric ions in the tetrahedral and octahedral sites and their concentrations in the composition are directly responsible for all these supreme phenomena. That's why these materials are widely used in preparing many electromagnetic devices like inductors, phase shifter, electromagnetic wave absorbers, memory devices etc. All these supreme properties can be changed by some parameters like synthesis technique, heat treatment, doping effect, frequency variation, purity of the reactants etc[1-3].

Rare earth materials in the universe are those materials that have some extraordinary properties of their own. When these rare earth materials are doped in any composition, it causes a drastic change in magnetocrystalline anisotropy, magnetostriction, magnetocaloric effect, magnetic moment etc. due to their localized nature of 4f electrons being totally screened by 5s and 5p orbital[4]. A famous and remarkable observation of the characterizations of ferrite compositions is the substitution of various divalent cation with any other element of the ferrite composition. In this regard, the substitution of rare earth material with any other element of the ferrite causes spectacular variations in structural, electrical and magnetic properties of the composition[3,4]. Many works regarding the rare earth materials substitution on ferrite materials were done and provided a lot of information of the consequence of rare earth materials doping[5-9].

Our previous study presented the effect of Yttrium (Y) substitution on structural and transport properties of Ni-Zn ferrite, where the X-ray diffraction pattern was discussed in brief and frequency dependent permeability and dielectric properties were investigated elaborately[10]. The aim of the present investigation is to demonstrate the detailed X-ray diffraction pattern, Scanning Electron Micrograph and M-H curves of Y^{3+} substituted Ni-Zn ferrite symbolized as $Ni_{0.25}$ $Zn_{0.75}Y_xFe_{2-x}O_4$ [x= 0.00, 0.02, 0.04, 0.06 and 0.08].

II. Sample Preparation

The Y^{3+} substituted Ni-Zn ferrite were synthesized using conventional solid state reaction method where analytical grade powder of NiO, ZnO, Y_2O_3 and Fe_2O_3 with purity of ~ 98% were taken as reactant. The method deals with grinding, calcination, sintering etc. At first all the reactants were taken in a mortar for crushing, grinding as well as milling with appropriate homogenization for 6 hours. Then all the samples were carried out for calcination at 850^{o}C. The calcined powders were crushed again to prepare fine powders. Then the pellet shaped samples were prepared using die-punch assembly of Hydraulic press by applying uniaxial pressure of 20MPa. The pellet shaped samples were taken for sintering operation at 1150^{o}C for 3 hours in order to bond the particles together with sufficient strength as well as to densify the grain compacts by eliminating the pores and thus to complete the reactions left unfinished in the calcination step.

All the samples were then carried out for various characterizations. The X-ray diffraction pattern for both undoped and Y doped samples were found by Philips X'pert pro powder X-ray diffractometer. The detail of surface morphology was observed by Scanning Electron Microscope (SEM). The field dependent magnetization as well as Hysteresis loops of all the samples were found from Vibrating Sample Magnetometer (Model: EV-9, MicroSense LLC, USA).

III. Results and Discussion

Structural Analysis

The structural phenomenon including phase identification, site occupancy etc. are shown in X-ray diffraction pattern of

*Author for correspondence. e-mail: *probal.phy@gmail.com*

$Ni_{0.25}$ $Zn_{0.75}Y_xFe_{2-x}O_4$ [*x*= 0.00, 0.02, 0.04, 0.06 and 0.08] in Fig. 1(a). Expected crystallization along with well-defined peaks are found for both undoped and Y doped specimens. The indexed XRD planes are found at (111), (220), (311), (222), (400), (422), (333), (440). It is clear from here that, all the indices are either even or odd which confirms the evolution of fcc type cubic spinel structure[11,12]. The small secondary peak of $YFeO_3$ can be found for the Y^{3+} doped samples from x = 0.06-0.08 that are presented as * in Fig. 1(a). The formation of unexpected secondary phase is due to its chemical kinetics of its formation[13,14] while preparing by solid state reaction method.

The trend of left shifting of XRD peaks with the increase of Y^{3+} doping can be observed in XRD patterns. Fig. 1(b) exhibits the shifting of (311) plane to the left direction from the position of the peak of undoped sample. Basically, this plane shifting occurs maybe due to the change in chemical composition or due to strain as well as d-spacing i.e., lattice parameter[15]. This lattice parameter was determined by applying Nelson- Riley function (N-R function) denoted as F(q)[16], where

$$F(q) = \frac{1}{2}\left(\frac{\cos^2 q}{\sin q} + \frac{\cos^2 q}{q}\right) \quad (1)$$

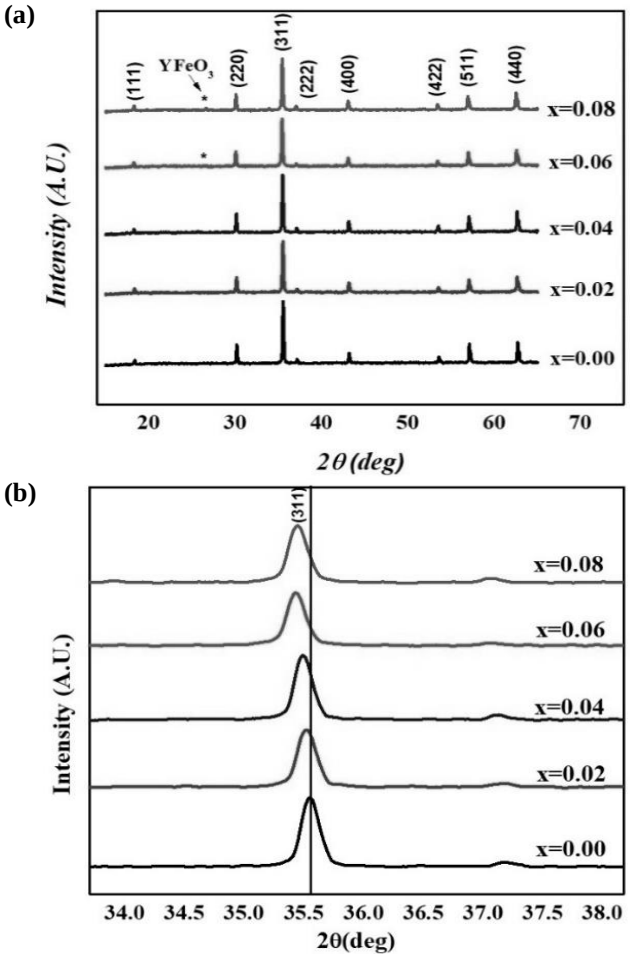

Fig. 1. (a) The XRD patterns for x= 0.00, .0.02, 0.04, 0.06 and 0.08; (b) The X-ray shifting of (311).

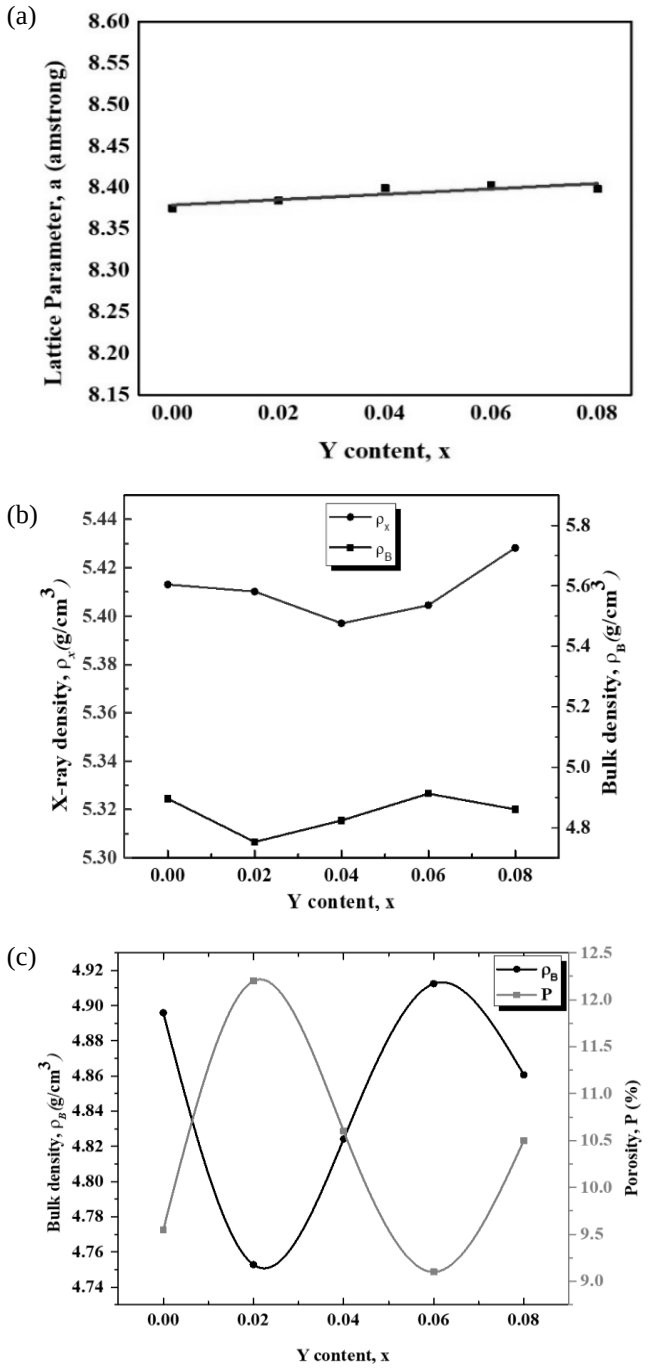

Fig. 2. Variation of (a) lattice parameter, (b) X-ray density vs. Bulk density and (c) Bulk density vs. Porosity of $Ni_{0.25}Zn_{0.75}Y_xFe_{2-x}O_4$ [x= 0.00, 0.02, 0.04, 0.06 and 0.08].

The variation of lattice parameter with respect to the concentration of Y^{3+} element is shown in Fig. 2(a). It can be seen here that, with the increase of Y^{3+} doping peaks shift toward the left direction and the lattice parameters show increasing tendency. Here the ionic radius of Y^{3+} (0.1011 nm) is quite greater than the ionic radius of Fe^{3+} (0.063 nm) which may be responsible for the left shifting of XRD peaks[15,16] and this angle shifting is a clear indication of the shrinkage of unit cell volume of the Y doped samples.

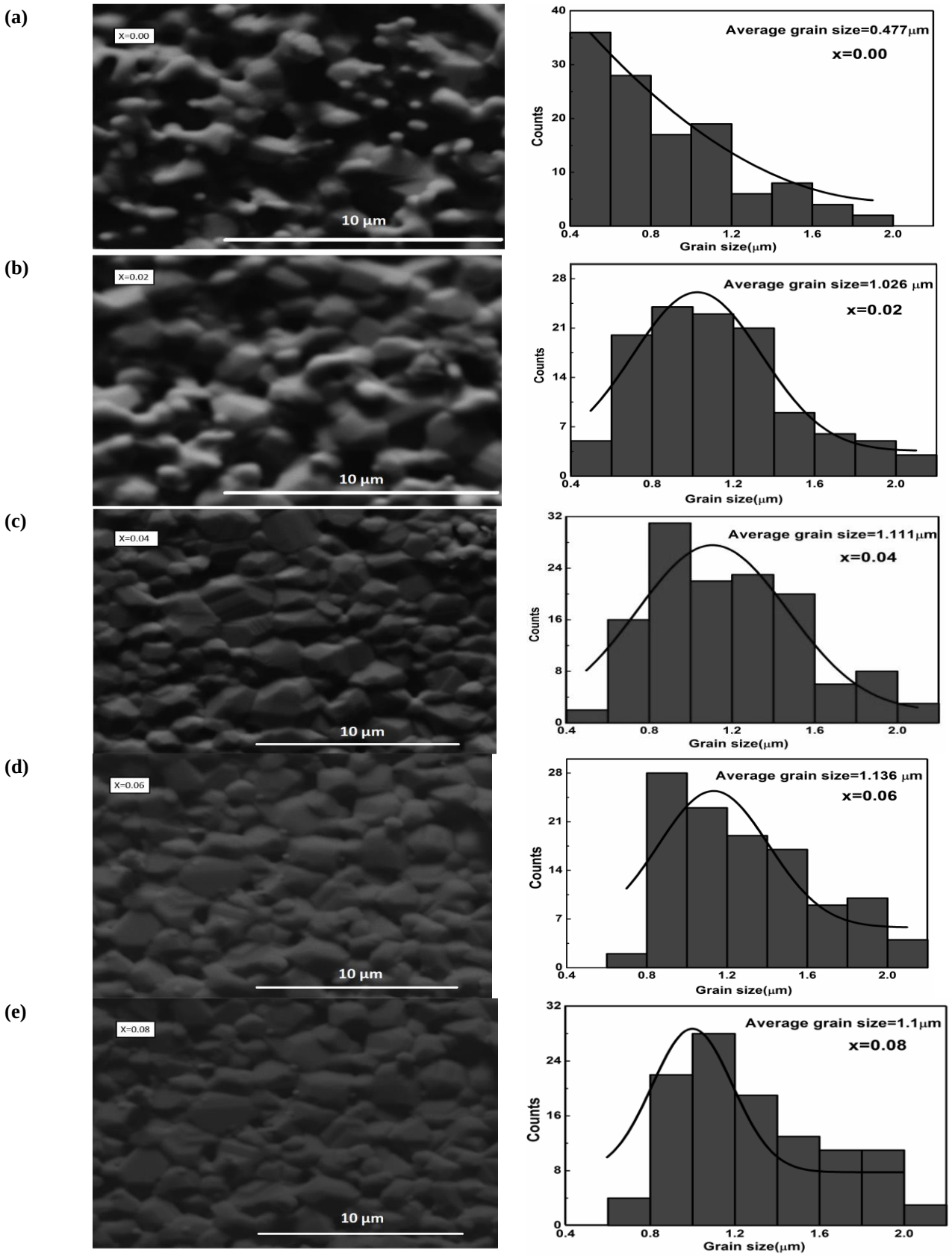

Fig. 3. SEM micrographs and the respective histograms of $Ni_{0.25}Zn_{0.75}Y_xFe_{2-x}O_4$ [(a) x = 0.00, (b) x=0.02, (c) x=0.04, (d) x=0.06 and (e) x=0.08] composites sintered at 1150 °C temperature.

The variation of bulk density (ρ_B) and X-ray density (ρ_x) are presented in Fig. 2(b). Basically, the bulk density was observed by following the usual mass and dimensional consideration whereas the X-ray density is the observation that was found from the molecular weight and volume of each sample. The porosity (P) or void fraction is a measure of the empty spaces in a material which is inevitable during the process of sintering of oxide materials. The respective equation for ρ_B, ρ_x and P are provided below[17]

$$\rho_B = \frac{m}{V} = \frac{m}{\pi r^2 h} \quad (2)$$

and $$\rho_x = \frac{8M}{na^3} \quad (3)$$

and $$P = \left(1 - \frac{\rho_B}{\rho_x}\right) \times 100\% \quad (4)$$

Initially, ρ_x shows the decreasing phenomenon and after a while it increases. This variation of ρ_x is analogous to the inverse relation with the variation of Bulk density. The ρ_B initially decreases and then starts to increase which is similar as the inverse relation of the variation of porosity that is shown in Fig 2(c). This observed decreasing tendency of ρ_B in 2% Y-doped sample may have resulted due to the irregular grain growth[18]. Whereas, the significance difference in atomic weights of initial iron and substituted yttrium cations (Y^{3+} (83.906 amu) > $Fe3^+$ (55.845 amu)) may have caused the increase of ρ_B in 4% and 6% Y-doped samples. Again, during the densification process, grain growth starts stimulating discontinuously and thus, the inter-granular porosity is diminished. This may have contributed toward the increase of bulk density and consequently caused the decrease in porosity.

Morphological Studies

The surface morphology, microstructure and hence the average grain size distribution of $Ni_{0.25}Zn_{0.75}Y_xFe_{2-x}O_4$ with various amounts of Y^{3+} were carried out using SEM imaging. The SEM micrographs and their corresponding histograms of all the samples reflect a clear role of Y^{3+} substitution on modifying grain size and it also demonstrated a dense microstructure marked with little trapped porosity compared to the microstructure of undoped sample (x=0.00). As observed from Fig. 3(a) the average grain size of undoped sample was measured to be ~ 0.477 µm. Substitution x= 0.02 of Y^{3+} at Fe- site within Ni-Zn ferrites improved its surface morphology with increased average grain size of 1.026 µm. The SEM image of this compound also reveals that the microstructure is dense enough but contains non-uniform grains, indicating polycrystalline nature of this composition. On further increment of Y^{3+} substitution up to x=0.06 concentration in Ni-Zn ferrites, the grain size (Fig. 4) of the samples continues to increase but then it starts to decrease for x=0.08 substitution.

In this study, the sintering temperature of the synthesized ferrites is much lower compared to the melting temperature of Y_2O_3 which is 2410 °C. Because of this huge difference in melting point and the sintering temperature, the replacement of Fe^{3+} ions in B-sites by Y^{3+} ions increase the metallic ion vacancies in vicinity so as to balance the electric charges near the grain boundary region. Consequently, this behavior makes it easier for the ions to diffuse and therefore speed up the grain boundary movements which results in promoting the grain growth[19, 20]. Moreover, it was demonstrated in an earlier investigation that the introduction of Y^{3+} ions induces the appearance of yttrium iron garnet (YIG) structure which assembles near the grain boundary region as solid solution. This behavior leads to the enhancement of oxygen vacancies which can perform as the material transportation path for the further advancement of the grain sizes in ferrites[21].

The existence of secondary phase of $YFeO_3$ as formerly observed from XRD patterns is clearer here in all the SEM micrographs which illustrate the presence of small particles that are segregated at the grain boundaries and formed a continuous phase surrounding the grains.

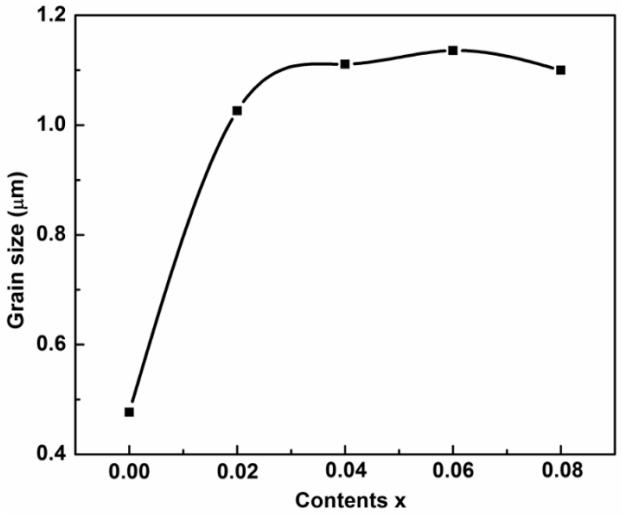

Fig. 4. The variation of grain size with the increasing Y substitution.

Magnetic Characterization

To inspect various magnetic phenomena like saturation magnetization (M_s), coercivity (H_c) and remanent magnetization (M_r) the hysteresis loops were taken for both undoped and Y^{3+} doped samples by applying maximum field of 10 kOe. In our investigation, according to Fig. 5, all the samples have shown well saturated hysteresis loops which indicates the existence of soft ferromagnetism behavior in undoped and Y-doped $Ni_{0.25}Zn_{0.75}Y_xFe_{2-x}O_4$ crystals. The influence of Y^{3+} substitution causes remarkable changes on these magnetic parameters that are shown in Table 1. From Table 1, it is distinctly visible that for the undoped sample with x=0.00 the saturation magnetization is found to be 42 emu/g and the remanent magnetization is 4 emu/g, which are highest among all the samples. In a recent study, the initially observed values of M_s and M_r (for undoped sample) have shown this similar decrement with the increasing Mn doping in $Ba_{0.4}Ca_{0.4}Sr_{0.2}Mn_xTi_{1-x}O_3$ crystal[22]. Another investigation

conducted by Nahar et al. on La^{3+} doped Cu-Zn Ferrite reported that with the increasing doping (La^{3+}) element all the magnetic parameters start to decrease[17]. These observations suggest that the magnetization in Y-doped composites is hard to realize since the spontaneous magnetization of the specimens comes from unbalanced antiparallel spin and that give rise to net spins other than those induced from the structural distortion[22].

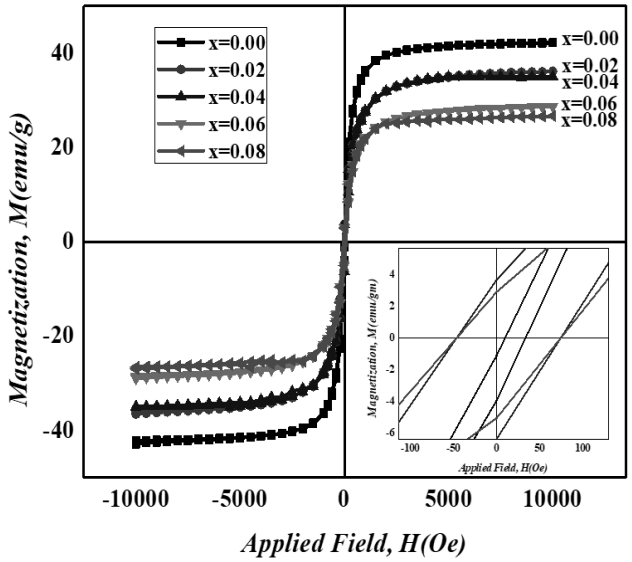

Fig. 5. Hysteresis loops (M-H curve) of $Ni_{0.25}Zn_{0.75}Y_xFe_{2-x}O_4$ [*x*= 0.00, 0.02, 0.04, 0.06 and 0.08].

Table 1. Saturation magnetization (M_s), coercivity (H_c) and remanent magnetization (M_r) of $Ni_{0.25}Zn_{0.75}Y_xFe_{2-x}O_4$, [x = 0.00, 0.02, 0.04, 0.06, and 0.08] ferrites sintered at 1150°C holding time 3 hours.

Content x	M_s (emu/g)	H_c (Oe)	M_r (emu/g)
0.00	42	42	4
0.02	36	36	4
0.04	35	35	4
0.06	28	28	3
0.08	27	26	3

However, the coercivity H_c also exhibits same decreasing phenomenon. All samples exhibited low coercivity in the range of ~27 to 42 Oe values indicating that all the samples belong to the family of soft ferrites. In general, the coercivity is linearly dependent on the magnetic anisotropy and de-magnetization factor. The decrease in coercivity with the increasing Y^{3+} is maybe due to the increase of grain boundaries which may cause the leading of a rise in pinning sites for the spins and therefore reduces coercivity[23]. This magnetization process is connected with soft magnetic behavior of magnetic material. The slow process of magnetization toward the saturation value is connected with the magnetic anisotropy effect[24-26]. Conventionally, doping accompanies grain growth and that is responsible for the decreases of magnetization due to the decrease of Fe content. There is a large change in the magnetic state due to cation distribution. The superexchange interaction between iron ions in tetrahedral and octahedral sites leads to the ordering in magnetic moment[25].

III. Conclusion

Polycrystalline $Ni_{0.25}Zn_{0.75}Y_xFe_{2-x}O_4$, [x = 0.00, 0.02, 0.04, 0.06 and 0.08] composites were synthesized by conventional solid-state reaction method and sintering process was carried out at 1150°C for 3 hours. The XRD patterns demonstrate the formation of fcc type cubic spinel structure with the existence of secondary phase for 6 to 8% Y doped (x=0.06-0.08) samples. The SEM micrographs of all the samples provide the information that the grain size increases with the increase of Y^{3+} doping. The field dependent hysteresis curves ensure the formation of ferromagnetic behavior for all the samples. With Y^{3+} doping, the variation of the distribution of Fe^{3+} in various sites, magnetocrystalline anisotropy, grain size, crystal defects, imperfection in lattice etc. may be responsible for the variation of saturation magnetization (M_s), coercivity (H_c) and remanent magnetization (M_r).

Acknowledgements

The authors are acknowledging The Solid State Physics Laboratory, Department of Physics, Khulna University of Engineering & Technology with Highest admiration. Moreover, the laboratory assistance of Materials Science Division, Atomic Energy Centre, Dhaka is also acknowledged with deepest sense of gratitude.

Reference

1. Nakamura, T., 1997. Low-temperature sintering of NiZnCu ferrite and its permeability spectra. *Journal of Magnetism and Magnetic Materials*. **168**(3), 285-291.
2. Akhter S., D. P. Paul, M. A. Hakim, D. K. Saha, H. N. Das, A. Parveen, and B. Anjuman., 2018. Transport Properties of Polycrystalline Mixed Copper-Zinc Ferrites. *Materials Research.* **21**(4), 1-6.
3. Ateia, E., M. A. Ahmed, and A. K. El-Aziz, 2007. Effect of rare earth radius and concentration on the structural and transport properties of doped Mn–Zn ferrite. *Journal of magnetism and magnetic materials.* **311**(2), 545-554.
4. Tahar, L. B., M. Artus, S. Ammar, L. S. Smiri, F. Herbst, M-J. Vaulay, V. Richard, J-M. Grenèche, F. Villain, and F. Fiévet, 2008. Magnetic properties of $CoFe_{1.9}RE_{0.1}O_4$ nanoparticles (RE= La, Ce, Nd, Sm, Eu, Gd, Tb, Ho) prepared in polyol. *Journal of Magnetism and Magnetic Materials.* **320**(23), 3242-3250.
5. Zhao, L., H. Yang, X. Zhao, L. Yu, Y. Cui, and S. Feng, 2006. Magnetic properties of $CoFe_2O_4$ ferrite doped with rare earth ion. *Materials Letters.* **60**(1), 1-6.
6. Sattar, A. A., A. H. Wafik, K. M. El-Shokrofy, and M. M. El-Tabby, 1999. Magnetic properties of Cu–Zn ferrites doped with rare earth oxides. *Physica status solidi (a).* **171**(2), 563-569.
7. Ateia, E., M. A. Ahmed, and A. K. El-Aziz, 2007. Effect of rare earth radius and concentration on the structural and

transport properties of doped Mn–Zn ferrite. *Journal of magnetism and magnetic materials.* **311**(2), 545-554.

8. Ahmed, M. A., N. N. Okasha, and M. M. El-Sayed, 2007. Enhancement of the physical properties of rare-earth-substituted Mn–Zn ferrites prepared by flash method. *Ceramics International.* **33**(1), 49-58.

9. Nayek, C., A. Tamilselvan, Ch Thirmal, P. Murugavel, and S. Balakumar, 2014. Origin of enhanced magnetization in rare earth doped multiferroic bismuth ferrite. *Journal of Applied Physics.* **115**(7), 073902-073906.

10. Akhter, S., P. Roy, M. A. Hossain, M. N. I. Khan and S. S. Sikder, 2019. Influence of Yttrium substitution on structural and transport properties of Ni-Zn () ferrite. *Journal of Engineering Science.* **10**(1), 45-50.

11. Shil, S. K., R. C. Sinha, Hakim, A. K. M., & Sikder, S. S. (2013). Influence of composition and sintering temperature on complex permeability of spinel type ni-zn ferrite. *Journal of Engineering*. **4**(1), 119-125.

12. Vucinic-Vasic, M., E. S. Bozin, L. Bessais, G. Stojanovic, U. Kozmidis-Luburic, M. Abeykoon, B. Jancar, A. Meden, A. Kremenovic, and B. Antic, 2013. Thermal evolution of cation distribution/crystallite size and their correlation with the magnetic state of Yb-substituted zinc ferrite nanoparticles. *The Journal of Physical Chemistry C*. **117**(23), 12358-12365.

13. Anwar, A., M. A. Basith, and S. Choudhury, 2019. From bulk to nano: A comparative investigation of structural, ferroelectric and magnetic properties of Sm and Ti co-doped BiFeO3 multiferroics. *Materials Research Bulletin.* **111**, 93-101.

14. Godara, P., A. Agarwal, N. Ahlawat, and S. Sanghi, 2015. Crystal structure refinement, dielectric and magnetic properties of Sm modified $BiFeO_3$ multiferroic. *Journal of Molecular Structure.* **1097**, 207-213.

15. Mostafa, M., M. J. Rahman, and S. Choudhury, 2019. Enhanced dielectric properties of $BaTiO_3$ ceramics with cerium doping, manganese doping and Ce-Mn co-doping. *Science and Engineering of Composite Materials.* **26**(1),62-69.

16. Vijatovićpetrović, M. M., J. D. Bobić, R. Grigalaitis, B. D. Stojanović, and J. Banys, 2013. La-doped and La/Mn-co-doped Barium Titanate Ceramics. *Acta Physica Polonica, A.* **124**(1).

17. Nahar, K., M. A. Hossain, P. Roy, M. N. I. Khan, and S. S. Sikder, 2020. Study of the Structural, Magnetic and Transport properties of La 3+ Doped Cu-Zn Ferrite. *Journal of Scientific Research*, 12(3), 259-267.

18. Mondal, P. K., M. A. Hossain, M. N. I. Khan, and S. S. Sikder, 2019. Structural, magnetic and transport properties of Samarium (Sm) doped Cu-Zn ferrites. *International Journal of Physical Science.* **14**(3), 21-29.

19. Su, H., H. W. Zhang, X. L. Tang, and Y. Shi, 2009. Effects of tungsten trioxide addition and top-temperature sintering period on properties of high-permeability NiCuZn ferrite. J. *Alloys Compd.* **468**, 290–294.

20. Su, H., H. W. Zhang, X. L. Tang, Y. L. Jing, 2007. Effects of MoO_3 and WO_3 additives on densification and magnetic properties of highly permeable NiCuZn ferrites. *Mater. Chem. Phys.***102**, 271-274.

21. Xing, Q., Z. Peng, C. Wang, Z. Fu, and X. Fu, 2012. Doping effect of Y^{3+} ions on the microstructural and electromagnetic properties of Mn–Zn ferrites. *Physica B* **407**, 388–392.

22. Anwar, A., A. Akter, and M. N. I. Khan, 2020. Influence of Mn^{2+} substitution on Structural, Morphological, Electrical and Magnetic properties of $Ba_{0.4}Ca_{0.4}Sr_{0.2}Mn_xTi_{1-x}O_3$ perovskites. *AIP Advances* **10**, 045307-045317.

23. Akhtar, M. N., M. Yousaf, S. N. Khan, M. S. Nazir, M. Ahmad, and M. A. Khan, 2017. Structural and electromagnetic evaluations of YIG rare earth doped (Gd, Pr, Ho, Yb) nanoferrites for high frequency applications. *Ceramics International.* **43**(18), 17032-17040.

24. Din, M. F., I. Ahmad, M. Ahmad, M. T. Farid, M. Asif Iqbal, G. Murtaza, Majid Niaz Akhtar, I. Shakir, M. F. Warsi, and M. A. Khan, 2014. Influence of Cd substitution on structural, electrical and magnetic properties of M-type barium hexaferrites co-precipitated nanomaterials. *Journal of Alloys and Compounds.* **584**, 646-651.

25. Ali, A. I., M. A. Ahmed, N. Okasha, M. Hammam, and J. Yeog Son, 2013. Effect of the La^{3+} ions substitution on the magnetic properties of spinal Li-Zn-ferrites at low temperature. *Journal of Materials Research and Technology.* **2**(4), 356-361.

26. Din, M. F., I. Ahmad, M. Ahmad, M. T. Farid, M. Asif Iqbal, G. Murtaza, Majid Niaz Akhtar, I. Shakir, M. F. Warsi, and M. A. Khan, 2014. Influence of Cd substitution on structural, electrical and magnetic properties of M-type barium hexaferrites co-precipitated nanomaterials. *Journal of Alloys and Compounds* **584**, 646-651.